



Deciphering the potent application of nanobentonite and $\alpha\text{-Fe}_2\text{O}_3$ /bentonite nanocomposite in dye removal: revisiting the insights of adsorption mechanism

Pratibha Sharma¹ · Vandana Yadav¹ · Sujata Kumari¹ · Debasree Ghosh¹ · Pooja Rawat² · Ankush Vij³ · Chandramohan Srivastava¹ · Sonia Saini⁴ · Vivek Sharma⁴ · Md. Imtaiyaz Hassan⁵ · Sudip Majumder¹ 

Received: 9 March 2021 / Accepted: 2 June 2021 / Published online: 9 June 2021
© King Abdulaziz City for Science and Technology 2021

Abstract

Clays are widely accepted for dye removal from wastewater. Here, in this work, nanobentonite was synthesized by a simple, rapid, and cost-effective chemithermal method. Additionally, nanobentonite was coupled with hematite nanoparticles via thermal coupling to prepare a nanocomposite with enhanced surface absorption. Surface morphology, compositional and structural analysis of synthesized samples were done using various characterization techniques. Results suggested that nanobentonite and nanocomposite having an average diameter of 35.36 and 21.85 nm respectively were synthesized. Nanocomposite exhibited increased surface area. Additionally, the ability of all samples as an adsorbent for removal of methylene blue (MB) and Congo red (CR), from an aqueous solution was investigated under various optimization conditions. Adsorption kinetics revealed that Pseudo II order equation fits well for the adsorption process following intraparticle diffusion mechanism for both the dyes. The adsorption equilibrium data of MB and CR was fitted well by the Langmuir and Freundlich adsorption isotherm model, respectively. The thermodynamic parameters suggested adsorption process is endothermic and spontaneous in nature with increased entropy value.

Keywords Bentonite clay · Acid activation · Nanocomposite · Dye degradation · Adsorption studies

Introduction

In effluents, the presence of dyes is one of the major concerns because of their adverse effects on many forms of life (Bulut and Karaer 2015). The discharge of dyes into the environment is important to be looked after for both

esthetical and toxicological reasons (Raffatulah et al. 2010; Santhi and Manonmani 2011). Wastewaters are the major contributors of colored effluents released from the industries like textile, printing, food coloring, dyeing, papermaking, cosmetics, etc. (Wang et al. 2011). Releasing even a small amount of dye in the water produces carcinogenic and mutagenic effects and thus affects aquatic life and the food webs (Liu et al. 2010). Thus it becomes environmentally important to remove these dyes from wastewater effluents (Chen and Huang 2010). Azo dyes are the most common dyes used for dyeing silk, cotton, and wool and can cause adverse health issues to both animals and humans (Raffatulah et al. 2010; Ghosh and Bhattacharyya 2002; Tan et al. 2008). Therefore, the treatment of effluents containing such dyes is of great concern because of its harmful impacts on receiving waters. Conventional methods of treatment such as precipitation, coagulation and flocculation, electrochemical destruction, photocatalytic oxidation, ozonation, biological treatment, and adsorption are developed for water decontamination applications (Santhi and Manonmani 2011; Huang et al. 2011). Adsorption is found to be the most efficient

✉ Sudip Majumder
sudip22m@gmail.com

- ¹ Department of Chemistry, Amity School of Applied Sciences, Amity University Haryana, Amity Education Valley, Manesar, Gurugram 122413, India
- ² Department of Applied Physics and Institute of Natural Sciences, Kyung Hee University, Yong-In, Gyeong-gi 17104, Republic of Korea
- ³ Department of Physics, School of Engineering, University of Petroleum and Energy Studies, Dehradun 248007, India
- ⁴ Department of Chemistry, Banasthali University, Banasthali 304022, India
- ⁵ Center for Interdisciplinary Research in Basic Sciences, Jamia Millia Islamia, New Delhi 110025, India

method for wastewater treatment because of its low cost, simplicity in operation, flexibility, and insensitivity to toxic pollutants (Raffatulah et al. 2010; Huang et al. 2011; Tran et al. 2010). For the removal of different types of dyes, there various types of adsorbents such as activated carbons, plant or lignocellulosic wastes, clays and biopolymers have been used (Raffatulah et al. 2010; Ngah et al. 2011; İşlek et al. 2008; Zanjanchi et al. 2011).

Bentonite is an excellent adsorbent and henceforth it is used for wastewater treatment and purification from oil, phenol, solvent, detergents, and heavy metal ions (Beall 2003; Neaman et al. 2003). Bentonite is often used as a fabricating material of organo-clay compounds due to its high adsorption power, large surface area, and good ion-exchange property. Recently, some groups of researchers have successfully attempted the synthesis of bentonite nanostructures using various approaches, though surprisingly the numbers are very limited. However, there are reports for the synthesis of bentonite nanostructure using sonochemical and solvothermal methods (Darvishi and Morsali 2011a, b). The synthesis of bentonite nanostructure can be very useful considering the larger surface area, higher adsorption capacity of nanomaterial that might lead to significant enhancement of properties compared to bulk bentonite. Moreover, the adsorption capacity of clays can be further enhanced using surface modification. One such modifications include the surface coating of clay with metal oxide nanoparticles. The extremely fine size of these nanoparticles impregnated over the surface of clay and yields favorable characteristics imparting an increase in surface area and altering basic properties (Motshekga et al. 2013; Sonawane et al. 2017; Lubis et al. 2019; Hashem 2013).

Here, in this article, we report a rapid and economical procedure for the synthesis of nanobentonite (NB) and α -Fe₂O₃/bentonite nanocomposite (FEB) using a chemothermal and thermal coupling method, respectively. Different structural and functional properties were investigated using several characterization techniques. The research work is also concerned with the investigation of the reactivity comparison of NB and FEB with bulk bentonite (B) in the removal of cationic non-azo dye methylene blue (MB) and anionic azo dye Congo red (CR) as model pollutant. The removal of both the dyes was studied in batch experiments optimizing different parameters. Adsorption isotherms are studied to indicate the mechanism of adsorption and estimate the maximum adsorption capacity and correlation coefficients. Adsorption kinetics are studied to determine the adsorption rate and mechanism of adsorption along with thermodynamic parameters.

Materials and methods

All the commercially available chemicals were used as received without any further purification.

Synthesis of hematite (α -Fe₂O₃) nanoparticles

Ferrous sulphate salt (Fe₂SO₄·7H₂O) (5 g, purchased from CDH) was dissolved in 100 mL distilled water and stirred at 60 °C for 30 min, followed by the addition of 50 mL liquor ammonia (pH ≈ 11) for precipitation of nanoparticles. The final product was filtered, washed with distilled water and ethanol, dried and then obtained reddish-brown powder was muffled at 600 °C for 3 h.

Synthesis of nanobentonite

A suspension of bentonite powder (5 g, purchased from Merck) in distill H₂O (100 mL) was made, followed by addition of 50 mL of concentrated HCl (pH ≈ 4). The reaction mixture was refluxed at 65 °C for 2 h with continuous stirring. Subsequently, the solution was filtered and the precipitate was washed thoroughly using distill H₂O and ethanol to remove the excess acid. The product was dried and then calcinated at 400 °C for 3 h. A whitish powder of bentonite nanoparticles (NB) were obtained.

Synthesis of α -Fe₂O₃/bentonite nanocomposite

Hematite nanoparticles were added to bulk bentonite in 1:2 ratio while activating it using acid following the same procedure of synthesizing nano bentonite. A brownish powder was obtained as a nanocomposite.

Absorbance studies

Absorption experiments were performed using MB and CR dye stock solution of 40 mg/L by preparing it in distilled water. All the batch experiments were carried out on a shaker incubator with constant stirring of 200 rpm using a known quantity of adsorbent and adsorbate and this mixture was stirred for fixed time intervals in dark at room temperature. The residual dye concentration in supernatant liquid obtained after centrifugation was determined spectrophotometrically at $\lambda_{\text{max}} = 664$ nm and at 500 nm for MB and CR dye respectively using UV–Visible spectrophotometer (UV Shimadzu 8450). Different experiments were carried out to study the effect of contact time, adsorbent dose, adsorbate dose, pH, and temperature. All the experiments were repeated thrice and the initial pH of solution was used throughout the experiments except for the one where the

initial pH of solution was estimated. Stock solution of dyes was prepared in double-distilled water (pH = 7.03). The percentage removal of dyes was estimated using relation as follows

$$\text{Dye removal (\%)} = (1 - C_t/C_o) \times 100,$$

where C_o and C_t was initial concentration and at time t .

pH variation effect

Effect of pH was studied using 100 mg of adsorbent dose dispersed in 100 mL of dye solution (40 mg/L). The pH of this solution was adjusted to 4–11 using NaOH (1 M) and HCl (1 M) solutions. The suspension was stirred at room temperature for fixed time interval, then aliquot (3 mL) was taken out and centrifuged. The supernatant was determined spectrophotometrically.

Adsorbent dose

The effect of adsorbent dosages was also studied by varying adsorbent doses from 25, 50, 100, 150, 200, 250 and 300 mg/L in 100 mL dye solution of fixed initial stock concentration of 40 mg/L. The mixture was stirred at room temperature for fixed time interval. Then 3 mL aliquot was taken out, centrifuged and supernatant was determined spectrophotometrically.

Adsorption isotherms study

The adsorption isotherms were studied by providing fixed adsorbent dosages (300 mg/L) as obtained from the adsorbent dose study to constant dye solution (100 mL) by varying initial dye concentration as 10, 40, 70, 90, 130, and 190 mg/L. The suspension was stirred at room temperature for fixed time period and then centrifuged. Subsequently, the supernatant containing residual dye concentration was measured spectrophotometrically and the amount of adsorbed dye was estimated using the following expression:

$$q_e = (C_o - C_e) \times V/m$$

where q_e (mg/g) was the amount of dye removed by nanoparticles at equilibrium. C_o and C_e (mg/L) was the initial and equilibrium concentration of dye, respectively. V (L) was the volume of dye solution under study and m (g) was the mass of adsorbent provided. The equilibrium data were fitted with Langmuir, Freundlich and Temkin isotherm models.

Adsorption kinetics study

To study adsorption kinetics and the mechanism involved for the removal of dyes, 100 mg of adsorbent was dispersed

in 100 mL of dye solution (40 mg/L) at room temperature for about 180 min. After fixed time intervals, aliquots of 3 mL were removed, centrifuged, and spectrophotometrically analyzed the concentration of dye in the supernatant. The amount of dye removed, q_t (mg/g) at time t (min) was calculated using following expression:

$$q_t = (C_o - C_t) \times V/m$$

where C_o and C_t (mg/L) were initial concentration and concentration of dye at time t , respectively; V (L) was the total volume of dye solution and m (g) was adsorbent dose. The kinetic of experiments was determined using Pseudo-I order and pseudo-II order reactions whereas the mechanism of adsorption was studied using Elovich, Reichenberg, and intraparticle diffusion model.

Thermodynamic effect

Effect of temperature was analyzed by adding 300 mg/L of adsorbent to 100 mL of dye solution agitating for fixed time interval at different temperatures (20, 28 and 35 °C) using initial pH and upto equilibrium time.

Characterization

Surface properties and compositional analysis

For the scanning electron microscopy (SEM) B, NB and FEB were suspended in 90% alcohol. A droplet of the suspension was transferred on a clean glass slide (1 cm × 1 cm) and micrographs were taken at a number of random locations with the help of Carl Zeiss SEM at an accelerating voltage of 15 kV after gold coating. Elemental analysis of samples was carried out using Energy Dispersive X-ray Spectroscopy (EDS). TEM analysis was done to study the morphology of nanocomposite where samples were mounted as a droplet of 1 mg/mL nanoparticle solution after 15 min sonication on a clean glass slide (1 cm × 1 cm) followed by gold coating. Micrographs were taken randomly at various perspective using TEM (Carl Zeiss, Germany) at an accelerating voltage of 15 kV. N_2 sorption analysis was done to evaluate Brunauer Emmett Teller (BET) surface area along with pore size distribution of all synthesized samples at 77 K using Quantachrome Autosorb IQ instrument. All samples were degassed before N_2 sorption analysis at 120 °C for 12 h. Zeta potential value and charge present at the surface of all the samples were evaluated via dynamic light scattering technique through zetasizer ver.7.11 (Malvern Instruments). A suspension of 1000 ng/mL in distilled water was prepared to determine zeta potential value by recording 12 zeta runs.

Structural characterisations

XRD measurements were done using a Model- Ultima-III Rigaku make (Japan) X-ray diffractometer with a Cu target slit 10 mm and using a Cu K α radiation of 1.54 Å wavelength. Scanning was done in a rate of 0.02°min⁻¹ in the region of 10° to 90° with a time constant of 2 min. For FTIR the samples were dried and ground with KBr pellets and analyzed on a Nicolet IR 200 (Thermo Electron Corp). The data was recorded in wavenumber range from 4000 to 400 cm⁻¹. Oxidation state of iron in Fe₂O₃ was determined by an Omicron Multiprobe Electron Spectroscopy System with Monochromated Al K α (1486.7 eV).

Results and discussions

Surface properties and compositional analysis

SEM-EDS

The surface morphology and microstructure of B, NB and FEB have studied using SEM (Fig. 1a-c). Figure 1a shows neat bentonite clay having a smooth surface with non-porous flakes and needle-like crystals. On acid activation of bentonite clay, particle size has reduced as shown in the inset of Fig. 1b. In Fig. 1c, the topography of nanocomposite

clearly showed a rough and porous surface due to impregnated hematite nanoparticles on NB surface (inset of Fig. 1c) that was added during acid activation of bentonite. This has also been confirmed from TEM images (Supplementary Fig. S1). This resulted in increased surface area of nanocomposite which has been confirmed using BET also in “[Brunner–Emmett–Teller analysis \(BET\) and zeta potential](#)” (Belachew and Bekele 2019).

Additionally, EDS has been performed to detect the composition of nanobentonite and its nanocomposite (Fig. 1d, e). It has revealed that both samples chiefly consist of Si and Al in their oxide form along with a trace amount of other cations. A very minute quantity of Cl has also been detected that surely came from initial HCl treatment (Bukit et al. 2013). The amount of iron also increased in the case of nanocomposite that proved its successful synthesis.

Brunner–Emmett–Teller analysis (BET) and zeta potential

The specific surface area and pore size distribution of all samples have been determined using adsorption–desorption of N₂ as reported in Fig. 2a. All the samples exhibited an H3 type hysteresis loop that supported the capillary condensation mechanism. At high relative pressure, the area enclosed within the hysteresis loop (type-IV) increased with an increase in surface area (Table 1). As expected nanocomposite possess the highest surface area among others

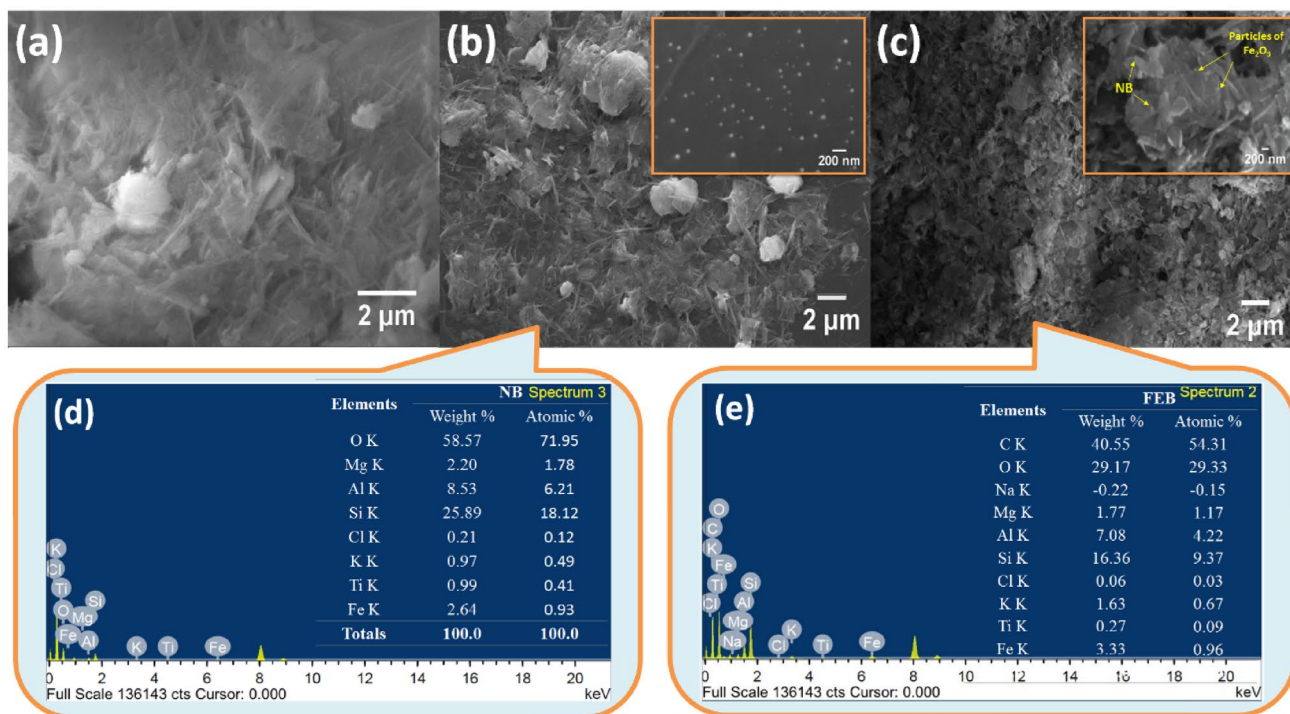


Fig. 1 SEM micrographs of B (a), NB (b) and FEB (c) (inset showing smaller scale images); and elemental composition of NB (d) and FEB (e)

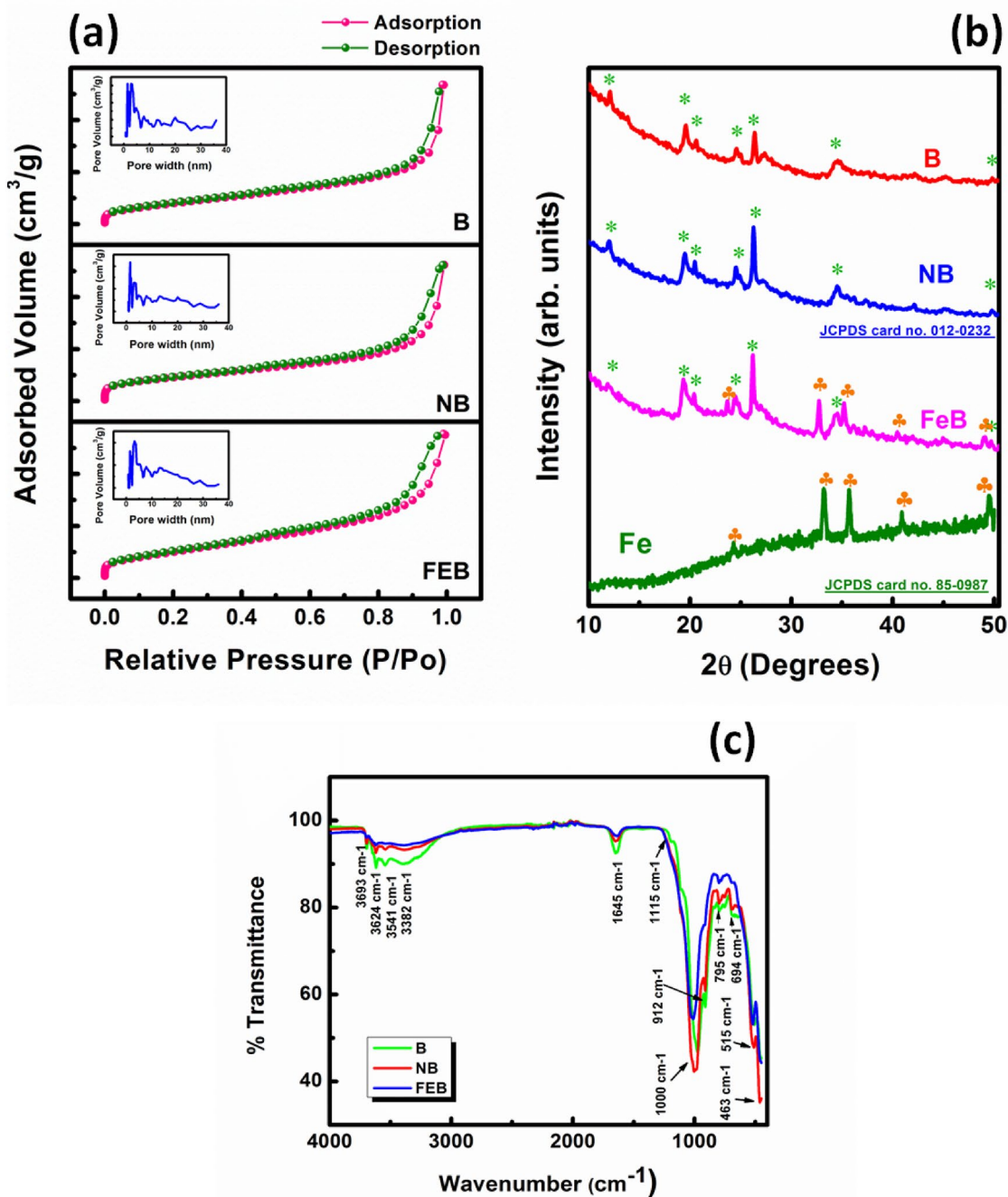


Fig. 2 **a** Hysteresis curve of N₂ sorption for B, NB and FEB, inset showing pore size distribution curve. **b** XRD pattern where all the reflections corresponding to bentonite clay and hematite nanoparticles are labelled with * and ♣, respectively and **c** FTIR spectra of all synthesized samples

that also supports our SEM and TEM micrographs (Mishra et al. 2017). This increase in surface area of NB and FEB resulted in their increased adsorption of dyes from wastewater as a potential application as discussed later in the manuscript. Additionally, on acid activation pore size distribution decreased as shown in the inset of Fig. 2a due to replacement of exchangeable cations like Na⁺, K⁺, and Ca⁺ by H⁺ supplied by acidic medium with simultaneous removal of

cations trapped in octahedral and tetrahedral sites like Al³⁺, Fe³⁺ and Mg²⁺ ions which also resulted in the somewhat whiter color of NB sample as compared to the bulk bentonite (Landoulsi et al. 2013). Whereas in nanocomposite some of these intraparticle pores have occupied by Fe³⁺ from hematite nanoparticles in place of H⁺ resulting in multiple pore size.

Table 1 Characteristic parameters of all samples

S. No	Properties	B	NB	FEB
1	Particle size (nm)	83.24 ± 4.16	35.36 ± 1.77	21.85 ± 1.09
	Strain	0.0082 ± 4.1E-4	0.0192 ± 9.6E-4	0.0310 ± 0.0015
	<i>d</i> -spacing (nm)	0.4527 ± 0.02	0.4522 ± 0.02	0.4513 ± 0.02
2	Specific BET surface area (m ² g ⁻¹)	154 ± 7.7	165 ± 8.25	197 ± 9.85
	Total pore volume (c cg ⁻¹) at <i>P/P_o</i> = 0.99	0.40 ± 0.02	0.41 ± 0.02	0.43 ± 0.02
	Pore size distribution (nm)	3.2 ± 0.16	1.44 ± 0.07	1.4 ± 0.07 and 2.9 ± 0.14
3	Zeta potential	- 21.3 ± - 1.06	- 23.0 ± - 1.15	- 23.1 ± - 1.15

Since the surface charge intensity also depended on the isomorphous substitution within the lattice. Hence, these structural changes also lead to a negative increment in the zeta potential value of NB and FEB as reported in Table 1. Moreover, with the decrease in particle size zeta potential values showed negative increment with increased colloidal stability (Sharma et al. 2021). According to our PXRD result, particle size decreased for NB and FEB as a result of this their zeta potential value also exhibited a negative increment suggesting that these nanoparticles exhibit good colloidal stability.

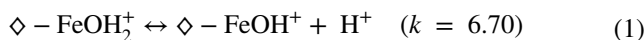
Structural characterisations

PXRD data suggested successful nanocomposite synthesis with the decrease in particle size and *d*-spacing values in NB and FEB along with an increase in the strain as shown in Table 1 and Fig. 2b resultant of distorted clay structure (Al-essa 2018; Sharma et al. 2019). FTIR also supported the XRD result and suggested distortion in tetrahedral and octahedral sites and leaching out of cations associated with them and thereby decrease in adsorbed moisture by these cations since the decrease in intensity of peaks corresponding to H-bonding has observed (Fig. 2c) (Ismaeel et al. 2017; Mishra et al. 2017). This resulted in an increase in adsorption sites with increased dye removal as discussed in “Adsorption studies” (Al-Essa 2018). All the characteristics peaks matched well with the literature as discussed in the supplementary information (de Oliveira et al. 2016; Mishra et al. 2017; Ismaeel et al. 2017; Salah et al. 2019; Belachew and Bekele 2019). For a detailed discussion of PXRD and FTIR refer to supplementary information. The oxidation state +3 for iron in hematite nanoparticles are also confirmed using XPS as reported in Supplementary information (Fig. S2) (Wang et al. 2019; Dhanasekaran et al. 2014).

Adsorption studies

pH variation effect

pH played a vital role in the adsorption capacity of dye onto nanoparticles due to electrostatic interactions between adsorbent and dye molecules. The initial pH has been evaluated by plotting dye removal (%) vs varying pH for 30 min as presented in Fig. 3a showed that, as expected, the adsorption of MB and CR dye onto all samples have favorable in alkaline and acidic environment, respectively. Moreover, among all the samples NB shows more affinity for the adsorption of MB dye with an adsorption capacity of 1.79 mg/g whereas FEB exhibits more adsorption affinity for CR dye having an adsorption capacity of 0.75 mg/g (supplementary Fig. S3a, b). This is because, in an alkaline environment, there have possibly more negative charges present on the bentonite surface due to protonation/deprotonation of hydroxy sites (M-OH) such as alumina. Therefore, the electrostatic attraction between the negatively charged adsorption site and the positively charged dye has enhanced, resulting in more cationic dye adsorbed on B and NB (Supplementary Fig. S4). Whereas, in an acidic medium, some of the available adsorption sites have occupied by protons competing with cationic dye leading to less adsorption. An opposite trend has been observed in the case of CR dye with more adsorption on the FEB surface that favored an acidic medium due to more availability of cationic adsorption sites. This has because in acidic medium hematite nanoparticles present on clay possess a positive charge due to surface hydrolysis of the hematite nanoparticles and the formation of FeOH⁺ as shown in Eqs. (1) and (2) and additionally -SiO and -Al₂OH of clay acts as acceptor groups (Supplementary Fig. S4) (Fu et al. 2004).



◆ are represented as the solid surface.

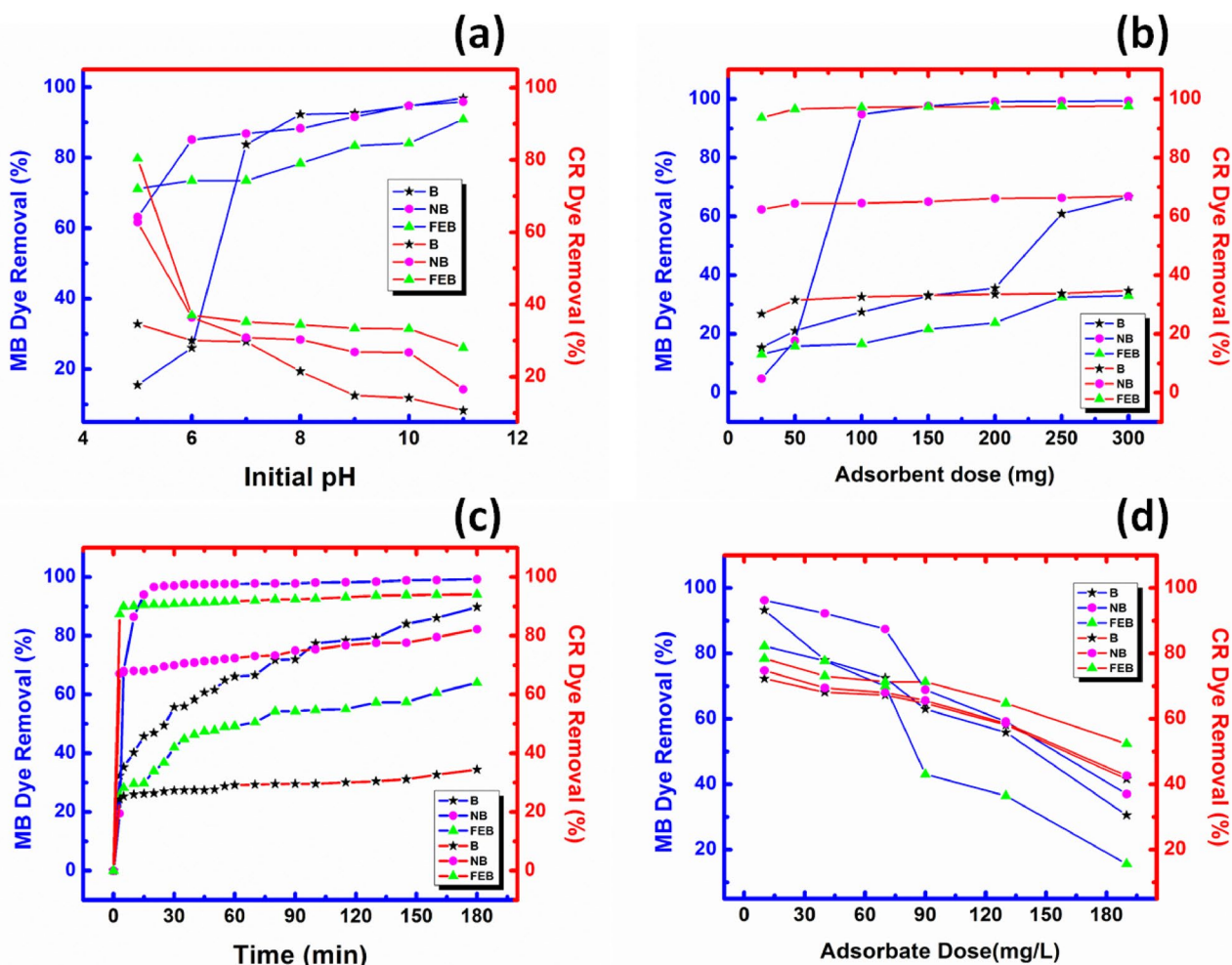


Fig. 3 Plots for Dye removal (%) for studying effect of pH (a), adsorbent dose (b), time (c), and adsorbate dose (d) using B, NB, and FEB as adsorbents and MB (blue color) and CR dye (red color) as adsorbate at room temperature

Hence, electrostatic interactions and hydrogen bonds are formed with donor groups of CR dye (Lubis et al. 2019; Alexander et al. 2019). Hence, for all the other batch experiments initial pH = 5 and 11 have used for CR and MB dye, respectively.

Effect of adsorbent dose

Figure 3b showed the effect of adsorbent dose on MB and CR dye studied using 20 mL of 40 mg/L dye solutions at initial pH for an equilibrium time of 30 min at room temperature. It has been observed that with the increase in adsorbent dosage percentage of dye removal has increased until an equilibrium state has reached due to more availability of adsorption sites. After that, the concentration of dyes removed becomes steady. With an increase in adsorbent dose, the percentage of MB dye removed are 33%, 99%, and 67% having the adsorption capacity of 0.78, 9.93, and

4.54 mg/L in FEB, NB, and B respectively whereas in CR dye, percentage of its removal has 98%, 67%, and 35% with adsorption capacity of 6.63, 3.57 and 1.85 mg/L in FEB, NB, and B, respectively (supplementary Fig. S3c, d). This is because an increase in adsorbent concentration provided a surface area for adsorption increased that implies more possible binding sites for dye molecules. Since some of these binding sites remain uncovered with increased adsorbent concentration that resulted in decreased value of adsorption capacity.

Effect of contact time

Figure 3c showed the progress of adsorption of dyes with respect to time using 300 mg/L of each adsorbent at initial pH at room temperature. Rapid initial uptake of both the dyes occurred resulting in setting up of equilibrium in less than 30 min. It has been observed that after 96% removal

of MB dye upto 20 min using NB an equilibrium state has established after that steady increase in dye removal is observed with a maximum of 99.33% of total dye removed from wastewater upto 180 min. On the other hand, B and FEB removed 90% and 64% of the total MB dye. In the case of CR dye, the equilibrium state has attained much earlier within 5 min followed by a steady increase in absorption of the dye. FEB removed a maximum of 94% of CR dye followed by 82% in NB and 34% in B upto 180 min. The adsorption capacity at equilibrium in MB dye is 0.76, 0.41, and 0.21 mg/g for B, NB, and FEB respectively whereas 0.10, 0.47, and 0.42 mg/g for B, NB, and FEB respectively for CR dye (Supplementary Fig. S3e, f). The initial high uptake of dyes is due to high adsorbate and adsorbent interactions with negligible solute–solute interaction and more availability of adsorption sites. But after equilibrium is attained mass transfer decreases and repulsion between adsorbate molecules on the surface and within the solution increases.

Effect of adsorbate dose

The effect of the initial concentration of adsorbate in solution has been studied by varying concentrations of both the dyes from 10 to 190 mg/L as reported in Fig. 3d at room temperature. This suggested that with an increase in the concentration of dyes, a decrease in total percentage removal of dyes has observed using 300 mg/L of adsorbent dose after 30 min of equilibrium time at initial pH. At lower adsorbate dose of 10 mg/L, B, NB, and FEB removed 93%, 96%, and 82% of MB dye whereas 72%, 75%, and 78% of CR dye respectively. An increase in adsorbate concentration to 190 mg/L B, NB, and FEB removed 30%, 37%, and 15% of MB dye whereas 41%, 42%, and 52% of CR dye. Moreover, the amount of dye adsorbed and percentage removal at 20, 28, and 35 °C as shown in the supplementary Fig. S5 suggested that initial dye concentration has a great impact on both the dyes. For example, at higher concentrations between 130 and 190 mg/L slight decrease in adsorption capacity has been observed (supplementary Fig. S5). This behavior change has been observed due to the chemisorption process that takes place at the adsorbent surface at the first region followed by the second adsorbate layer and a decrease in adsorption capacity by the third region perhaps due to dimerization of dyes at their higher concentration. Since the ionic nature of dyes played a vital role in surface chemical reactions with adsorbent accompanied by adsorption process (Almeida et al. 2009).

Study of adsorption isotherms

A relationship between the amount of adsorbate per unit mass of adsorbent at a specific temperature and its concentration at equilibrium is provided by adsorption isotherms. These isotherms describe how the adsorbate molecules are distributed between the liquid and solid phases at the equilibrium of the adsorption state. Several models can be used for isotherms and the analysis of isotherm data suggests which model is well accommodated that can be used for further consideration (Almeida et al. 2009). The equilibrium data of MB and CR are analyzed using Langmuir (Fig. 4a, b), Freundlich (Fig. 4c, d) and Temkin (Fig. 4e, f) equation to find out the suitable model and to understand the type of adsorption and interactions between adsorbate and adsorbent surface.

Langmuir isotherm In Langmuir Isotherm, the process accounts for the monolayer adsorption over a homogeneous adsorbent surface with the absence of any kind of interactions between adsorbate molecules. The Langmuir Isotherm linear form is expressed as follows:

$$\frac{C_e}{q_e} = \frac{1}{bq_{\max}} + \frac{C_e}{q_{\max}}$$

where C_e (mg/L) is the equilibrium concentration of the dye solution, q_e (mg/g) is the equilibrium capacity of adsorbed dye on the adsorbent. q_{\max} (mg/g) represented the maximum adsorption capacity of the adsorbent following monolayer formation and elucidates the maximum value of q_e that can be achieved with an increase in C_e . The b parameter is the Langmuir adsorption constant (L/mg) and is connected to the free energy of adsorption that can be increased by increasing the adsorption bond strength. The slope and intercept of the linear regression plot of (C_e/q_e) versus C_e are used to determine the values of b and q_{\max} (Fig. 4a, b). Additionally, another important parameter known as separation factor, R_L is calculated using $R_L = 1/1 + b(C_o)$ equation, where C_o is the initial adsorbate concentration of both the dyes. R_L value indicates the nature of adsorption as if the value of $R_L > 1$ means unfavorable adsorption if $R_L = 1$ indicates linear adsorption if $0 < R_L < 1$ indicates favorable adsorption and $R_L = 0$ means irreversible adsorption (Patil et al. 2016).

From Fig. 4a it is clear that MB dye fits well to a linear plot of the Langmuir model that explains the presence of monolayer formation of MB dye in the adsorption process on each adsorbent with a high value of correlation coefficient (R^2) as reported in Table 2. The high adsorption capacity of adsorbents has been indicated by Q_{\max} and K_F values from Langmuir and Freundlich isotherm, respectively (Table 2). Also, R_L values lie between 0 and

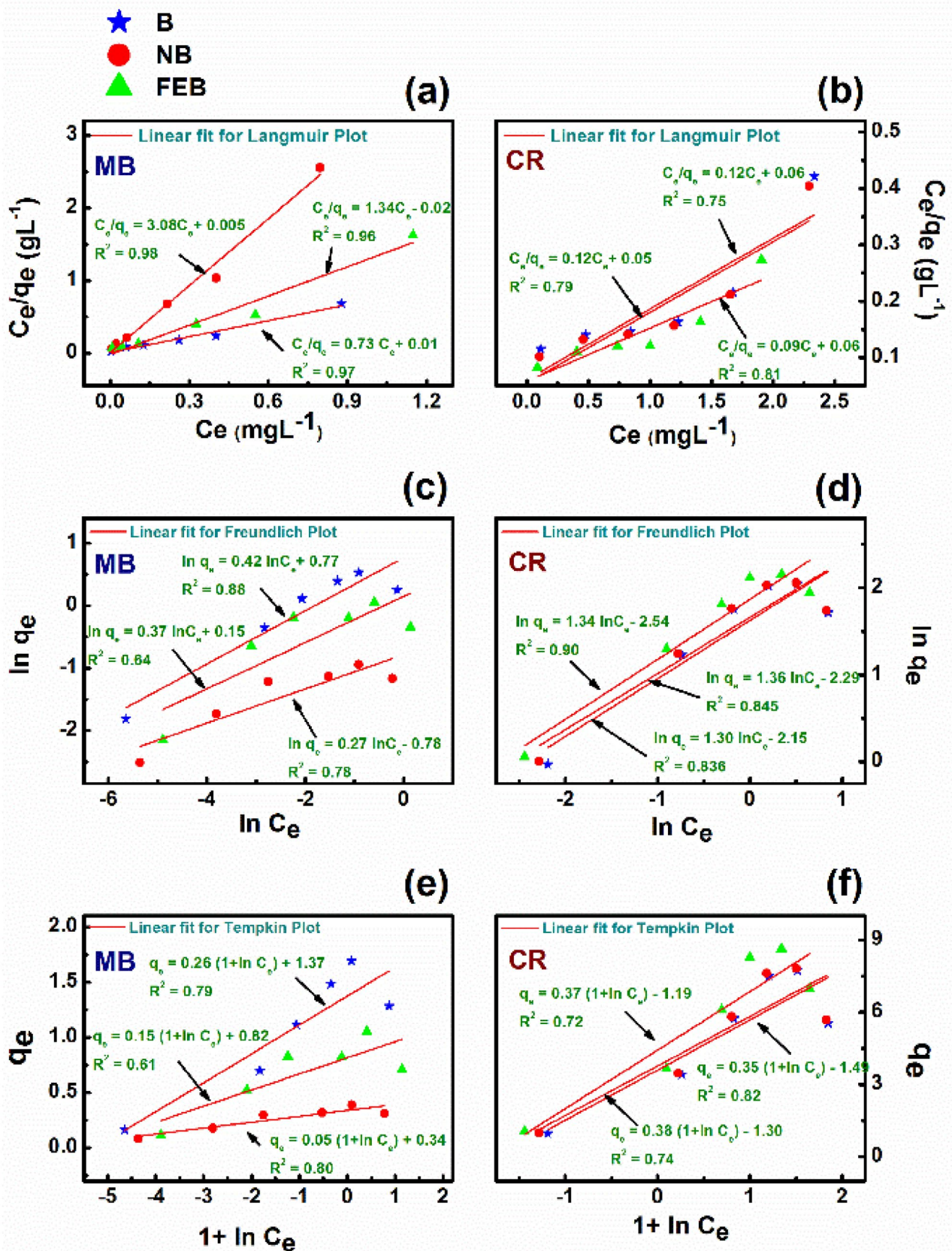


Fig. 4 Plots of Langmuir (a, b), Freundlich (c, d), and Temkin (e, f) adsorption isotherms for the adsorption of MB (a, c, e) and CR (b, d, f) dye on 300 mg/L of B, NB, and FEB at initial pH at room temperature

Table 2 Important parameters for adsorption isotherms

Experimental results			Langmuir model				Freundlich model			Tempkin model		
Dye	Sample	<i>T</i> (°C)	<i>R</i> ²	<i>K_L</i> (L/g)	<i>Q_{max}</i> (mg/g)	<i>R_L</i>	<i>R</i> ²	<i>K_F</i> (L/g)	1/ <i>n</i>	<i>R</i> ²	<i>K_T</i> (L/g)	<i>bt</i>
MB	B	20	0.98	56.89	0.79	4.78E−4	0.83	0.97	0.27	0.77	483.47	1316.25
		28	0.97	86.22	1.37	3.16E−4	0.88	2.15	0.42	0.79	190.96	888.88
		35	0.99	25.57	2.72	0.001	0.88	4.11	0.44	0.95	208.18	649.39
	NB	20	0.95	34.77	0.19	7.81E−4	0.65	0.26	0.21	0.55	1144.77	5459.42
		28	0.98	552.04	0.32	4.93E−5	0.78	0.46	0.27	0.80	574.08	4363.96
		35	0.99	604.62	0.45	4.50E−5	0.79	0.67	0.23	0.85	5066.41	5172.28
	FEB	20	0.93	13.11	0.53	0.002	0.80	0.54	0.28	0.81	334.04	2273.86
		28	0.96	72.66	0.74	3.74E−4	0.64	1.16	0.37	0.61	266.33	1592.03
		35	0.97	32.18	0.84	8.44E−4	0.52	1.37	0.29	0.45	532.74	1759.51
CR	B	20	0.72	2.16	8.22	0.012	0.80	5.52	0.69	0.66	5.71	74.76
		28	0.75	2.03	8.00	0.013	0.84	5.07	0.67	0.72	5.66	111.86
		35	0.79	3.66	7.78	0.007	0.79	6.16	0.63	0.66	7.79	134.69
	NB	20	0.72	1.84	9.08	0.014	0.82	5.83	0.71	0.72	5.51	70.73
		28	0.78	2.27	7.99	0.012	0.84	5.26	0.64	0.74	6.28	113.26
		35	0.80	2.30	9.66	0.011	0.85	6.87	0.67	0.79	7.09	120.34
	FEB	20	0.76	1.89	9.81	0.014	0.85	6.47	0.70	0.76	6.10	68.08
		28	0.81	1.61	10.64	0.016	0.90	6.48	0.69	0.82	6.21	95.86
		35	0.84	2.40	10.04	0.011	0.87	7.27	0.66	0.80	7.91	119.96

1 that indicated a favorable adsorption process (Table 2). Hence, adsorption of MB taken place over the homogeneous adsorbent surface of NB and B more than FEB with equally distributed adsorbate molecules over an identical and energetically equivalent available site with no interactions between adsorbed molecules. The Langmuir correlation coefficient also indicated that with an increase in temperature adsorption capacity increased for MB dye, whereas CR dye has not followed such a trend (Fig. 4b).

Freundlich isotherm It is very well accepted that Freundlich Isotherm followed multilayer adsorption considering the interaction between adsorbed molecules and is generally applied to a solid catalyst, heterogeneous in nature. The Freundlich equation in linear form is expressed as follows:

$$\log C_e = \log K_F + \frac{1}{n} \log C_e$$

where K_F shows the adsorbent capacity for the adsorbate and $1/n$ represents the dyes adsorption intensity on solid, it is a function of adsorption. K_F and n are dimensionless constants. The Freundlich Isotherm model (Fig. 4c, d) is appropriate for the adsorption on heterogeneous surfaces through reversible adsorption and uniform energy distribution. CR dye followed Freundlich isotherm as shown in Fig. 4d with maximum regression value of FEB that provided heterogeneous surface. The value of $1/n$ is a measure for surface heterogeneity or adsorption intensity that lied between 0 to 1. If the value of $1/n < 1$ than 1 then indicated

chemisorption, $1/n = 0$ indicated cooperative absorption, and approaching zero indicates heterogeneity (Patil et al. 2016). Results suggested Chemisorption from the value of $1/n$ with high adsorption capacity in FEB as reported in Table 2.

Temkin isotherm The Temkin Isotherm model considered the interaction between adsorbate and adsorbent that resulted in a linear decrease in isotherm considering the heat of adsorption of all molecules in the layer with coverage and uniform distribution of binding energies up to maximum is used for the adsorption characterization. The linear equation of Temkin is as follows:

$$Q_e = \beta \ln \alpha + \beta \ln C_e, \quad \text{where, } \beta = RT/b$$

α is the equilibrium constant relative to the maximum binding energy (L/g) and T is the absolute temperature in Kelvin. R is the universal gas constant (8.314 J/mol/K) and b is the Temkin constant which is related to the heat sorption (J/mg). The value of α and β are calculated from the slope and intercept of a plot between q_e versus $\ln C_e$. As observed from Fig. 4e, f none of the dyes follow the Temkin equation as this equation fits less to liquid phase equilibria and more relevant for the prediction of gas-phase equilibria. This is because in liquid phase phenomena observed are more complex since the adsorbed molecules are not organized in a tightly packed structure with identical orientation.

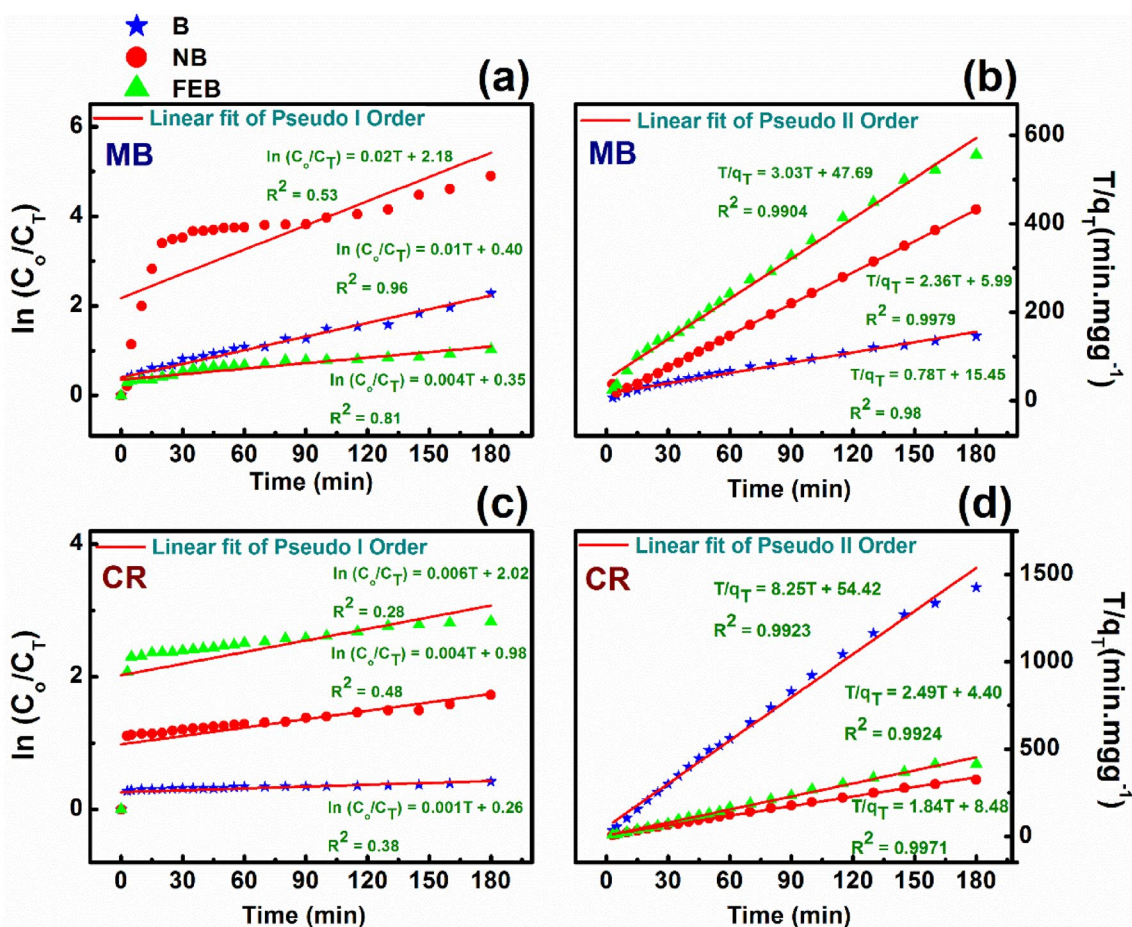


Fig. 5 Pseudo I order (a, c) and Pseudo II order (b, d) plots to study adsorption kinetics of MB (a, b) and CR (c, d) dye adsorbed over 1 g/L of B, NB and FEB at room temperature and using initial pH of mixture

Adsorption kinetics study

The adsorption kinetics is studied to evaluate the appropriate rate expression and adsorption mechanism. Adsorption kinetics has been studied by fitting Lagergren’s pseudo-first and Ho’s second-order model as represented in Fig. 5a–d. The adsorption mechanism has been concluded using Elovich, Reichenberg, and intraparticle diffusion model (Fig. 6a–f) as discussed in detail in the supplementary information. The linear form of pseudo-first-order reaction and pseudo-second-order reactions are shown in Eqs. (3) and (4) respectively.

$$\ln(Q_e - Q_t) = \ln Q_e - k_1 t \tag{3}$$

$$t/Q_t = 1/k_2 Q_e^2 + t/Q_e \tag{4}$$

where Q_e and Q_t are adsorption capacity (mg/g) of dye at equilibrium and at equilibrium time t (min), respectively.

k_1 and k_2 are rate constants for pseudo-first-order (min⁻¹) and pseudo-second-order (g/mg/min), respectively. From Fig. 5b, d, it has been observed that pseudo-second-order kinetic is well followed by both the dyes as observed from the values of correlation coefficient (R^2) reported in Table 3. Since pseudo-second-order model favored chemisorption between adsorbate and adsorbent molecules. Hence, the rate-limiting step is the several electronic interactions, cation exchange, or chemical bonding that played a vital role in the sorption process.

Additionally, the adsorption mechanism of dye adsorption as discussed in the supplementary information suggested that the intraparticle diffusion (or Weber and Morris) model (Fig. 6a, b) has been followed by both the dyes accompanied with Elovich and Reichenberg mechanism also. From Table 3, it has been concluded that Adsorption of MB over NB follows the Reichenberg (Fig. 6e) and B and FEB followed the Elovich model (Fig. 6c). For CR adsorption, FEB followed Elovich equation (Fig. 6d) rest B and NB followed

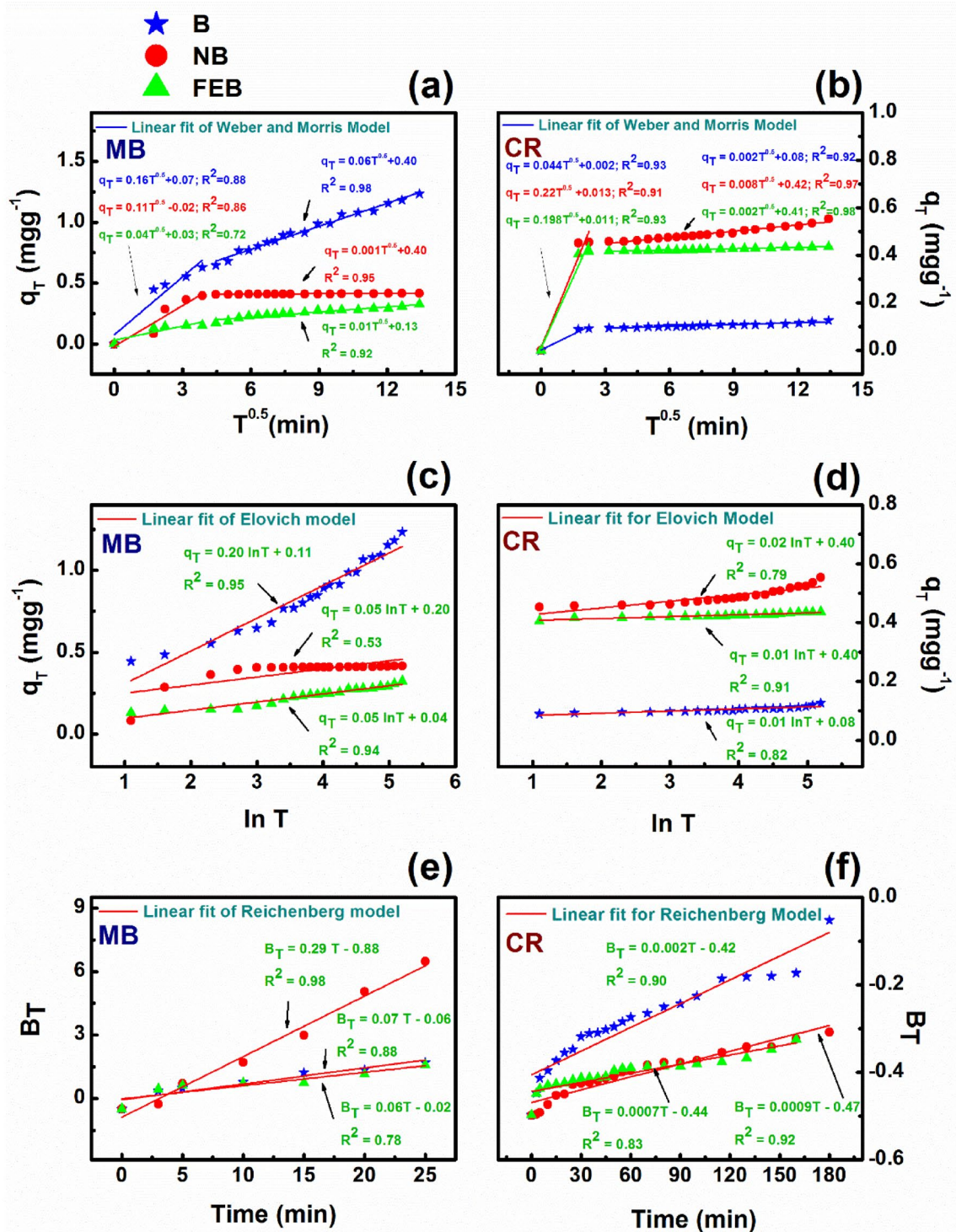


Fig. 6 Plots to study the mechanism of adsorption kinetics using Weber and Morris (a, b), Elovich (c, d), and Reichenberg (e, f) models for MB (a, c, e) and CR (b, d, f) dyes adsorbed over 1 g/L of B, NB and FEB at room temperature and using initial pH of the mixture

the Reichenberg equation (Fig. 6f). This suggested in FEB chemisorption occurred for sorption of adsorbate over adsorbent without desorption of products. Consequently, the rate

of adsorption decreases with time due to increased surface coverage.

Table 3 Important parameters for adsorption kinetics measured at room temperature using initial pH

Dye	Sample	Pseudo I order			Pseudo II order		
		Q_e (mg/g)	K_1 (min ⁻¹)	R^2	Q_e	K_2 (g/mg/min)	R^2
MB	B	1.49	0.0102	0.96	1.29	25.60	0.9839
	NB	8.83	0.018	0.53	0.42	1.07	0.9979
	FEB	1.42	0.0041	0.81	0.33	5.18	0.9904
CR	B	1.30	0.0009	0.38	0.12	0.80	0.9923
	NB	2.67	0.0042	0.48	0.54	2.51	0.9971
	FEB	7.56	0.0058	0.28	0.40	0.39	0.9924

Adsorption mechanism

Dye	Sample	Intra particle diffusion				Elovich model			Reichenberg model						
		Phase	K_i (mg/g min ^{1/2})	C	R^2	α	β	R^2	Intercept	R^2					
MB	B	I	0.1586	0.0735	0.88	0.34	5.00	0.95	- 0.06	0.88					
		II	0.0630	0.3995	0.99										
	NB	I	0.1116	- 0.0208	0.86						2.74	20.11	0.53	- 0.88	0.98
		II	0.0010	0.4017	0.95										
	FEB	I	0.0388	0.0292	0.72						0.12	19.96	0.94	- 0.78	0.78
		II	0.0140	0.1354	0.92										
CR	B	I	0.0441	0.0024	0.93	268.40	136.70	0.82	- 0.40	0.90					
		II	0.0026	0.0852	0.92										
	NB	I	0.2186	0.0135	0.92						1.22E6	44.05	0.79	- 0.47	0.92
		II	0.0089	0.4229	0.97										
	FEB	I	0.1985	0.0112	0.93						1.27E25	156.99	0.91	- 0.44	0.83

Table 4 Important thermodynamics parameters calculated by using 300 mg/L of adsorbent, varying initial dye concentration, at initial pH and varying temperature

Dye	Sample	dH (kJ/mol)	dS	dG (kJ/mol)
MB	B	231.43	23.72	- 776.92
	NB	1179.56	90.02	- 890.84
	FEB	440.86	45.42	- 603.91
CR	B	169.50	14.16	- 156.11
	NB	92.81	9.81	- 132.90
	FEB	66.21	8.03	- 118.58

Effect of temperature and thermodynamics study

Temperature is an important factor to decide the adsorptive capacity of dye onto the surface of the nanoparticles. Increasing the temperature resulted in an increase in the rate of diffusion of adsorbate molecules over the adsorbent surface or within the pores due to the reduced viscosity of the solution. Hence, the temperature-dependent study revealed the change in thermodynamic parameters such as Gibbs free energy (dG), change in enthalpy (dH), and entropy change (dS) accompanying adsorption of dyes using the von't Hoff equation.

$$\ln K_L = -dH/RT + dS/R \tag{5}$$

where R and T are ideal gas constant (8.314 J mol⁻¹ K) and temperature (K). K_L is the equilibrium constant of Von't Hoff equation. The values of thermodynamics parameters are calculated by linear plot between $\ln K_L$ and $1/T$ as shown in supplementary information Fig. S6 where slope and intercept gave the value of dH and dS respectively. Results suggested that with an increase in temperature adsorption capacity as well as percentage removal of dyes has increased as shown in Table 4. This is due to an increase in mobility of adsorbate molecules thereby facilitating more adsorption. Moreover, bentonite lattice possesses a positive thermal expansion coefficient so that activation in swelling effect within bentonite layers with an increase in temperature that induced more penetration of dye molecules (Almeida et al. 2009). The positive change in enthalpy value indicative of endothermic behavior with monolayer dye adsorption onto nanoparticles. The negative value of change in Gibbs free energy indicated spontaneous and highly favorable chemisorption which is also supported by adsorption kinetics data. The positive value for change in entropy suggests an increased degree of freedom on the irreversible sorption process. This could be explained using various explanations such as the release of hydrated inorganic cation from the adsorbent

surface, or any structural change as a result of adsorbate-adsorbent interactions or it could be due to increased solid-solution interface gained extra translational entropy when solvent molecules adsorbed over adsorbent is displaced by dye molecules (Almeida et al. 2009).

Conclusion

In this article, we presented a method of synthesizing small and uniform nanoparticles of Bentonite by a simple, rapid & cost-effective chemithermal route. Additionally, α -Fe₂O₃/bentonite nanocomposite was prepared to enhance the adsorption rate of bentonite. Surface studies using SEM and TEM suggested the successful formation of nanocomposite where hematite nanoparticles were adsorbed over bentonite surface which was also supported by EDS that confirmed an increased percentage of Fe in the nanocomposite. PXRD and FTIR suggested that acid activation of bulk bentonite and formation of nanocomposite resulted in decreased particle size and crystallinity due to distortion of octahedral and tetrahedral sites with leaching out of interstitial cations associated with them exposing edges of clay with more absorption sites. BET result also supported this by showing increased specific surface area. Zeta potential values also suggested the formation of stable colloidal particles with decreased zeta potential values. Additionally, all the samples were studied for removal of MB and CR dye from wastewater that suggested 99.33% of MB and 94% of CR dye were successfully removed by NB and FEB, respectively at room temperature. The adsorption kinetic studies show that the removal of MB and CR is a rapid process and the adsorption process obeyed the pseudo-second-order model following intraparticle diffusion mechanism where boundary layer formation is the rate-determining step following chemisorption. It was found that the experimental isotherm data can be fitted well to the Langmuir equation for MB dye and Freundlich equation for CR dye. The removal of MB and CR dye favors NB and FEB, respectively. The study on the adsorption mechanism shows that the adsorption of dyes on all the samples was dominated by cation exchange and electrostatic interaction between adsorbate and adsorbent. Adsorption of both the dyes was endothermic and spontaneous in nature with increased entropy. Overall, our nanocomposite enhanced the adsorption capacity of bentonite for even anionic dyes that was not possible even on acid activation of bentonite due to electrostatic repulsions between negative charges present over-dye and bentonite surface. Hence, our nanocomposite could be successfully used for the removal of dyes from wastewater.

Supplementary Information The online version contains supplementary material available at <https://doi.org/10.1007/s13204-021-01927-z>.

Acknowledgements PS, and SM would like to thanks Amity University, Haryana for supporting this work. SM would like to acknowledge the support provided under the DST-FIST Grant No.SR/FST/PS-I/2019/68 of Govt. of India.

Declarations

Conflict of interest The authors declare that there was no conflict of interest in this work.

References

- Al-Essa K (2018) Activation of Jordanian bentonite by hydrochloric acid and its potential for olive mill wastewater enhanced treatment Khansaa. *J Chem*. <https://doi.org/10.1155/2018/8385692>
- Alexander JA, Zaini MAA, Surajudeen A, Aliyu ENU, Omeiza AU (2019) Surface modification of low-cost bentonite adsorbents—a review. *Part Sci Technol* 37:538–549. <https://doi.org/10.1080/02726351.2018.1438548>
- Almeida CAP, Debacher NA, Downs AJ, Cottet L, Mello CAD (2009) Removal of methylene blue from colored effluents by adsorption on montmorillonite clay. *J Colloid Interface Sci* 332:46–53
- Beall GW (2003) The use of organo-clays in water treatment. *Appl Clay Sci* 24:11–20. <https://doi.org/10.1016/j.clay.2003.07.006>
- Belachew N, Bekele G (2019) Synergy of magnetite intercalated bentonite for enhanced adsorption of congo red dye. *SILICON* 12:603–612. <https://doi.org/10.1007/s12633-019-00152-2>
- Bukit N, Frida E, Harahap MH (2013) Preparation natural bentonite in nano particle material as filler nanocomposite high density polyethylene (Hdpe). *Chem Mater Res* 3:13. www.iiste.org
- Bulut Y, Karaer H (2015) Adsorption of methylene blue from aqueous solution by crosslinked chitosan/bentonite composite. *J Dispers Sci Technol* 36:61–67. <https://doi.org/10.1080/01932691.2014.888004>
- Chen AH, Huang YY (2010) Adsorption of remazol black 5 from aqueous solution by the templated crosslinked-chitosans. *J Hazard Mater* 177:668–675. <https://doi.org/10.1016/j.jhazmat.2009.12.083>
- Darvishi Z, Morsali A (2011a) Synthesis and characterization of nano-bentonite by sonochemical method. *Ultrason Sonochem* 18:238–242
- Darvishi Z, Morsali A (2011b) Synthesis and characterization of nano-bentonite by solvothermal method. *Colloids Surf A Physicochem Eng Asp* 377:15–19. <https://doi.org/10.1016/j.colsurfa.2010.11.016>
- de Oliveira CIR, Rocha MCG, da Silva ALN, Bertolino LC (2016) Characterization of bentonite clays from Cubati, Paraíba (Northeast of Brazil). *Cerâmica* 62:272–277. <https://doi.org/10.1590/0366-69132016623631970>
- Dhanasekaran V, Anandhavelu S, Polychroniadis EK, Mahalingam T (2014) Microstructural properties evaluation of Fe₂O₃ nanostructures. *Mater Lett* 126:288–290
- Fu H, Quan X, Liu Z, Chen S (2004) Photoinduced transformation of gamma-HCH in the presence of dissolved organic matter and enhanced photoreactive activity of humate-coated alpha-Fe₂O₃. *Langmuir* 20(12):4867–4873. <https://doi.org/10.1021/la0364486> (PMID: 15984243)

- Ghosh D, Bhattacharyya KG (2002) Adsorption of methylene blue on kaolinite. *Appl Clay Sci* 20:295–300
- Hashem FS (2013) Removal of methylene blue by magnetite-covered bentonite nanoparticles. *Eur Chem Bull* 2:524–529
- Huang XY, Bu HT, Jiang GB, Zeng MH (2011) Cross-linked succinyl chitosan as an adsorbent for the removal of methylene blue from aqueous solution. *Int J Biol Macromol* 49:643–651. <https://doi.org/10.1016/j.ijbiomac.2011.06.023>
- İşlek C, Sinağ A, Akata I (2008) Investigation of biosorption behavior of methylene blue on *Pleurotus ostreatus* (Jacq.) P. Kumm. *Clean* 36:387–392. <https://doi.org/10.1002/clen.200700167>
- Ismaeel SH, Mabrouk MS, Ali AAA, Abn-Elwalead K (2017) Synthesis and characterization of bentonite nanocomposites from Egyptian bentonite clay. *Int J Nanotechnol Allied Sci* 1:16–29
- Landoulsi O, Megriche A, Calvet R, Espitalier F, Ferreira JMF, Mgaidi A (2013) Effects of heating and acid activation on the structure and surface properties of a kaolinite-illite-smectite clay mixture. *Open Miner Process J* 6:13–20. <https://doi.org/10.2174/1874841401306010013>
- Liu Y, Zheng Y, Wang A (2010) Enhanced adsorption of methylene blue from aqueous solution by chitosan-g-poly (acrylic acid)/vermiculite hydrogel composites. *J Environ Sci* 22:486–493. [https://doi.org/10.1016/S1001-0742\(09\)60134-0](https://doi.org/10.1016/S1001-0742(09)60134-0)
- Lubis S, Sheilatina S, Sitompul DW (2019) Photocatalytic degradation of indigo carmine dye using α -Fe₂O₃/bentonite nanocomposite prepared by mechanochemical synthesis. *IOP Conf Ser Mater Sci Eng* 509:012142. <https://doi.org/10.1088/1757-899X/509/1/012142>
- Mishra A, Mehta A, Sharma M, Basu S (2017) Enhanced heterogeneous photodegradation of VOC and dye using microwave synthesized TiO₂/clay nanocomposites: a comparison study of different type of clays. *J Alloys Compd* 694:574–580. <https://doi.org/10.1016/j.jallcom.2016.10.036>
- Motshekga SC, Ray SS, Onyango MS, Momba MNB (2013) Microwave-assisted synthesis, characterization and antibacterial activity of Ag/ZnO nanoparticles supported bentonite clay. *J Hazard Mater* 262:439–446. <https://doi.org/10.1016/j.jhazmat.2013.08.074>
- Neaman A, Pelletier M, Villieras F (2003) The effects of exchanged cation, compression, heating and hydration on textural properties of bulk bentonite and its corresponding purified montmorillonite. *Appl Clay Sci* 22:153–168. [https://doi.org/10.1016/S0169-1317\(02\)00146-1](https://doi.org/10.1016/S0169-1317(02)00146-1)
- Ngah WSW, Teong LC, Hanafiah MAKM (2011) Adsorption of dyes and heavy metal ions by chitosan composites : a review. *Carbohydr Polym* 83:1446–1456. <https://doi.org/10.1016/j.carbpol.2010.11.004>
- Patil SP, Bethi B, Sonawane GH, Shrivastava VS, Sonawane S (2016) Efficient adsorption and photocatalytic degradation of Rhodamine B dye over Bi₂O₃ -bentonite nanocomposites : a kinetic study. *J Ind Eng Chem* 34:356–363
- Raffatulah M, Sulaiman O, Hashim R, Ahmad A (2010) Adsorption of methylene blue on low-cost adsorbents: a review. *J Hazard Mater* 177:70–80. <https://doi.org/10.1016/j.jhazmat.2009.12.047>
- Salah BA, Gaber MS, Kandil AHT (2019) The removal of uranium and thorium from their aqueous solutions by 8-hydroxyquinoline immobilized bentonite. *Minerals* 9:626. <https://doi.org/10.3390/min9100626>
- Santhi T, Manonmani S (2011) Malachite green removal from aqueous solution by the peel of *Cucumis sativa* fruit. *Clean* 39:162–170. <https://doi.org/10.1002/clen.201000077>
- Sharma P, Dhiman S, Kumari S, Rawat P, Srivastava C, Sato H, Akitsu T, Kumar S, Hassan I, Majumder S (2019) Revisiting the physicochemical properties of hematite (α -Fe₂O₃) nanoparticle and exploring its bio-environmental application. *Mater Res Express* 6:095072. <https://doi.org/10.1088/2053-1591/ab30ef>
- Sharma P, Kumari S, Ghosh D, Yadav V, Vij A, Rawat P, Kumar S, Sinha C, Saini S, Sharma V, Hassan MI, Srivastava C, Majumder S (2021) Capping agent-induced variation of physicochemical and biological properties of α -Fe₂O₃ nanoparticles. *Mater Chem Phys* 258:123899. <https://doi.org/10.1016/j.matchemphys.2020.123899>
- Sonawane GH, Patil SP, Shrivastava VS (2017) Photocatalytic degradation of safranin by ZnO–bentonite: photodegradation versus adsorbability. *J Inst Eng Ser E* 98:55–63. <https://doi.org/10.1007/s40034-016-0089-1>
- Tan IAW, Ahmad AL, Hameed BH (2008) Adsorption of basic dye on high-surface-area activated carbon prepared from coconut husk: equilibrium, kinetic and thermodynamic studies. *J Hazard Mater* 154:337–346. <https://doi.org/10.1016/j.jhazmat.2007.10.031>
- Tran HV, Tran LD, Nguyen TN (2010) Preparation of chitosan/magnetite composite beads and their application for removal of Pb(II) and Ni(II) from aqueous solution. *Mater Sci Eng C* 30:304–310. <https://doi.org/10.1016/j.msec.2009.11.008>
- Wang H, Mao J, Zhang Z, Zhang Q, Zhang L, Zhang W, Li P (2019) Photocatalytic degradation of deoxynivalenol over dendritic-like α -Fe₂O₃ under visible light irradiation. *Toxins* 11:105
- Wang L, Zhang J, Wang A (2011) Fast removal of methylene blue from aqueous solution by adsorption onto chitosan-g-poly (acrylic acid)/attapulgite composite. *Desalination* 266:33–39. <https://doi.org/10.1016/j.desal.2010.07.065>
- Zanjanchi MA, Sajjadi H, Arvand M, Mohammad-Khah A, Ghalami-Choober B (2011) Modification of MCM-41 with anionic surfactant : a convenient design for efficient removal of cationic dyes from wastewater. *Clean* 39:1007–1013. <https://doi.org/10.1002/clen.201000350>

Publisher's Note Springer Nature remains neutral with regard to jurisdictional claims in published maps and institutional affiliations.